Control Engineering Practice 140 (2023) 105658

Contents lists available at ScienceDirect

Control Engineering Practice

journal homepage: www.elsevier.com/locate/conengprac

Condition-based Design of Variable Impedance Controllers from User Demonstrations

Alberto San-Miguel [*,a], Vicenç Puig [a], Guillem Alenyà [a]

Institut de Robòtica i Informàtica Industrial CSIC-UPC, Llorens i Artigas, 4-6, Barcelona 08028, Spain

ARTICLE INFO

Keywords:
Variable Impedance Control
Learning from Demonstration
Linear Parameter Varying

ABSTRACT

This paper presents an approach to ensure conditions on Variable Impedance Controllers through the off-line tuning of the parameters involved in its description. In particular, we prove its application to term modulations defined by a Learning from Demonstration technique. This is performed through the assessment of conditions regarding safety and performance, which encompass heuristics and constraints in the form of Linear Matrix Inequalities. Latter ones allow to define a convex optimisation problem to analyse their fulfilment, and require a polytopic description of the VIC, in this case, obtained from its formulation as a discrete-time Linear Parameter Varying system. With respect to the current state-of-art, this approach only limits the term definition obtained by the Learning from Demonstration technique to be continuous and function of exogenous signals, i.e. external variables to the robot. Therefore, using a solution-search method, the most suitable set of parameters according to assessment criteria can be obtained. Using a 7-DoF KinovaGen3 manipulator, validation and comparison against solutions with relaxed conditions are performed. The method is applied to generate Variable Impedance Controllers for a pulley belt *looping* task, inspired by the Assembly Challenge for Industrial Robotics in World Robot Summit 2018, to reduce the exerted force with respect to a standard (constant) Impedance Controller. These controllers fulfil a set of safety constraints, namely stability, bounds on task variables and maximum response overshooting; and their performance is determined by the User Preference heuristic, which allows to intuitively define the desired compliant behaviour along the task. In the context of the task, this is used to generate new controllers for one-off modifications of the nominal belt *looping* task setup without new demonstrations.

1. Introduction

Great research efforts are devoted to introduce robots in anthropic domains (both industrial and domestic) for the sake of further enhancing tasks by physically interacting with humans and the environment. This calls for techniques that, firstly, formalise task characteristics as structures such that, secondly, can be used by control strategies for execution. For the first part, Learning from Demonstrations (LfD) techniques allow the generation of task descriptions through multiple human-guided demonstrations, from which relevant information can be extracted Ravichandar et al. (2020). This approach is suitable for users that are not familiar with robotic platforms and does not require an iterative execution process until a successful solution is found as with Reinforcement Learning (RL) based techniques Kober et al. (2013). For the second part of the problem, Impedance Control (IC) schemes have arisen as a trade-off between classical position and force tracking control, such that the relationship between them is tracked instead Hogan (1985). This approach is especially relevant in those scenarios where the robot must follow a trajectory but physical interactions (with humans or the environment) might happen or are even necessary for task completion. Moreover, many tasks require or benefit from the modulation of impedance terms throughout the task, namely Variable Impedance Control (VIC) Ikeura and Inooka (1995). Therefore, there has been a recent interest in integrated solutions that make use of the LfD paradigm to generate modulation profiles for VIC terms Abu-Dakka and Kyrki (2020).

However, in this intersection of techniques, it is required to ensure the fulfilment of some conditions that determine a reliable execution of the task. In all application contexts, ensuring stability is the paramount concern. For VIC, on top of requiring positive terms as for IC, term modulations need to be considered for stability assessment. Many approaches in the literature make use of methods based on Lyapunov

* Corresponding author.:
E-mail address: asanmiguel@iri.upc.edu (A. San-Miguel).

https://doi.org/10.1016/j.conengprac.2023.105658
Received 3 February 2023; Received in revised form 31 July 2023; Accepted 3 August 2023
Available online 1 September 2023

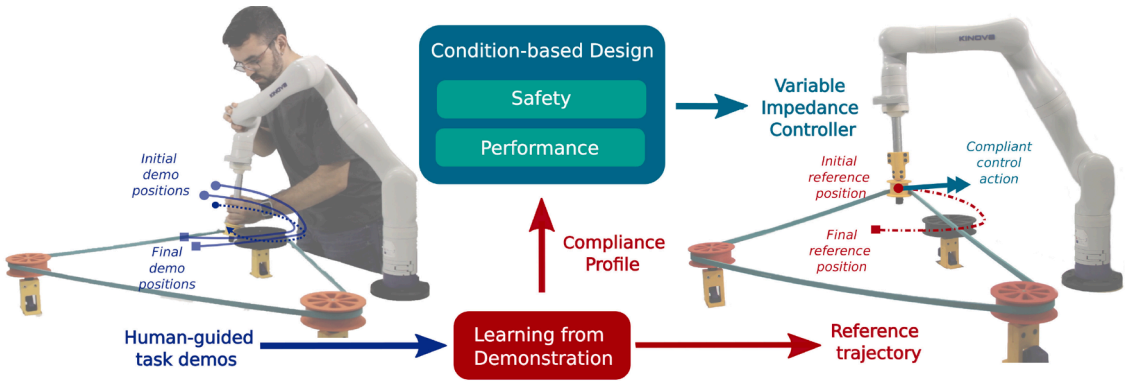

Fig. 1. From human-guided demonstrations, LfD is used to provide the reference trajectory to follow together with the required compliance profile for the task. This is used to define a Variable Impedance Controller, and the proposed approach (Condition-based Design) provides the set of parameters that complete its definition such that safety and performance conditions are fulfilled. The person appearing in this Figure is the first author and gave permission to use his image for this purpose.

theory, which proves stability through the existence of a suitable candidate function Behal et al. (2009). This has led to the derivation of sufficient conditions on modulation profiles (joint or individual) as in Kronander and Billard (2016). In this line, advances have been made in simplifying them through the imposition of particular structures for modulation terms, e.g. with an online filter as in Bednarczyk et al. (2020b). Other approaches consider energy-based strategies, e.g. through the so-called energy tanks Ferraguti et al. (2013) that "store" all the dissipative effects (energy-wise) for performing non-dissipative movements, which might be ill-posed by its dependency on robot state and initialization. Within LfD context, Linear Quadratic Regulator (LQR)-based approaches are usually chosen to set desired compliant behaviour Calinon et al. (2014); Medina et al. (2012). The approach presented in Khansari et al. (2014) defines stability conditions (for pre-defined forms of term modulations) and discusses its compatibility with the use of learning techniques, which was shown afterwards in Khader et al. (2020). Besides stability, up to our knowledge, only a few works addressing standard IC consider the introduction of other conditions, e.g. Bednarczyk et al. (2020a), but without addressing its joint use with LfD techniques.

In this paper, we contribute with a systematic framework to simultaneously guarantee multiple conditions on VICs by offline tuning its parameters. Particularly, we put the focus on those obtained from a LfD technique to extract a compliance profile, expanding our previous work San-Miguel et al. (2022). Conditions can limit an operation region for the controller, i.e. aimed at safety (e.g. stability), or determine how its operation suits the desired behaviour for the task, i.e. aimed at performance. For those defined as constraints, VIC operation is embedded by a polytopic description generated through its formulation as a Linear Parameter Varying (LPV) system, which w.r.t. state-of-art approaches, only limits modulations to be continuous and function of exogenous signals to the robot. Moreover, this description is given for its discrete-time form to acknowledge controller implementation in the real robot, which is executed in a fixed-frequency control loop. Conditions are arranged into an assessment problem such that the most suitable set of parameters that makes VIC fulfil them is generated. Figure 1 conceptualises the proposed approach for the chosen LfD technique in the context of the case study presented in this work, consisting of a pulley belt *looping* task to generate VIC that reduce required force w.r.t. constant IC. Moreover, a new heuristic is presented as a performance condition to intuitively set the desired compliant behaviour, namely User Preference, which in task context is used to generate new controllers for on-off modifications of the setting. In comparison with other techniques used to render compliant behaviours such as LQR, User Preference heuristic links better to the desired compliance as it is characterised through two parameters that only shape stiffness parameter.

The paper is organised as follows: Sect. 2 details the VIC description used to exemplify the method, based on the well-known LfD technique presented in Calinon et al. (2010). Section 3 details the procedure to obtain the polytopic description for the VIC from LPV formulation. The assessment process is described in Sec. 4 including chosen conditions on safety and performance. Section 5 portraits the complete method integrating the VIC description generation from demonstrations and the iterative assessment together with the solution-search method. Design validation experiments have been included in Sec. 6 and its application for the case study in Sec. 7. Finally, conclusions on the method are drawn in Sec. 8 together with a discussion on the results and future work.

2. Problem Statement

For the sake of simplicity, let's consider a 1-DoF task. Impedance Control (IC) aims at imposing a second-order dynamic relationship between (external) force $F(t)$ and system motion. For a trajectory tracking task, it is represented by the position error $e := p^r(t) - p(t)$ and its derivatives, w.r.t. a reference trajectory $\{p^r, \dot{p}^r, \ddot{p}^r\}_{t=0}^{T}$. Thus, the IC relationship is characterised by a set of terms that leverage motion variables, namely inertia H (for acceleration), damping D (for velocity) and stiffness K (for position). As aforementioned, Variable Impedance Controllers (VICs) vary these terms to change robot behaviour throughout a task. In this paper, the focus is put on a VIC with time-variant stiffness

$$H\,\ddot{e}(t) + D\,\dot{e}(t) + K(t)\,e(t) = F(t). \tag{1}$$

In this work, LfD is used to generate the modulation profile for $K(t)$. Particularly, through the well-known parametrization presented in Calinon et al. (2010), which links variance in position over different demonstrations for the same trajectory to the required compliance. Thus, lower variability, i.e. small position differences at the same time, will require lower compliance, i.e. high stiffness. For this purpose, a Heteroscedastic Gaussian Process (H-GP) model is considered to embed all the demonstrations and extract the required data. In comparison with the approach in Calinon et al. (2010), GPs have been chosen since they have less parameters to be tuned, and capturing correlation is not needed as VIC is stated for an individual DoF. This model consists of two standard GP models: one on the mean of the observations and another on the variance between observations, i.e. $\mathcal{N}(\boldsymbol{\mu}(t), \boldsymbol{\Sigma}(t))$. Thus, H-GP can be generated through Expectation-Maximization (EM) on the data set $\mathcal{D} = \{\{(t_{m,n}, p^d_{m,n})\}_{n=1}^{T_n}\}_{m=1}^{M}$ conformed of a set of M position demonstrations p^d_n aligned for times t_n of size T_m, as presented in Kersting et al. (2007). From this description, reference trajectory is described by the mean, i.e. $\mu(t) = p^r(t)$, and $\dot{p}^r$ and $\ddot{p}^r$ obtained through differentiation, and eigenvalues $\lambda(t)$ of the inverse covariance matrix $\boldsymbol{\Sigma}^{-1}(t)$ are used to define the

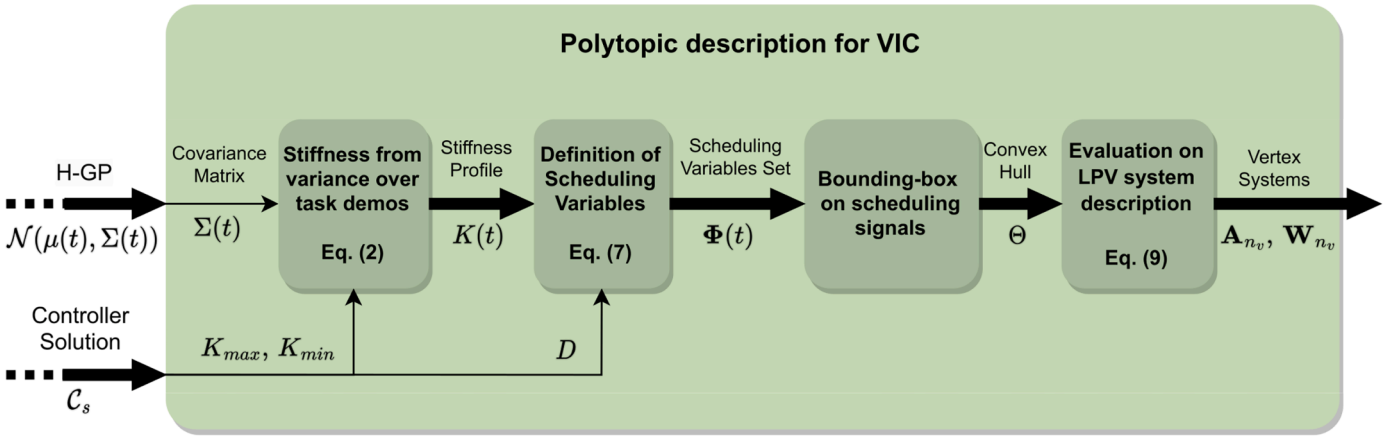

Fig. 2. Generation of the polytopic description of the VIC from controller solution and the H-GP model embedding task demonstrations.

variant stiffness K as a function of time as

$$K(t) = K_{\min} + (K_{\max} - K_{\min}) \frac{\log(\lambda(t)) - \log(\lambda_{\min})}{\log(\lambda_{\max}) - \log(\lambda_{\min})}. \tag{2}$$

Considering this, a controller solution $\mathscr{C}_s$ can be defined as the tuple of parameters that unequivocally determine the behaviour of (1). Assuming H is given beforehand:

$$\mathscr{C}_s = \langle K^s_{\max},\ K^s_{\min},\ D^s \rangle. \tag{3}$$

where the superscript "s" denotes that variables correspond to a controller solution tuple. The method presented in this paper aims at finding the most suitable $\mathscr{C}_s$ such that the VIC fulfils a set of conditions regarding safety and performance.

At this point, it is important to note that, although a 1 - DoF controller is presented, the method is not limited to a particular number nor a certain combination of DoFs. Also, it should be mentioned that we make use of this particular LfD technique to showcase our approach with a well-understood compliance generation paradigm. Instead, the proposed approach can be applied to any other technique that generates modulation profiles (function of continuous exogenous signals) and simultaneously modulates any of the parameters. These topics will be further discussed in Sec. 8.

3. Polytopic description for VIC

Some of the conditions imposed for the VIC require to consider its complete operation range, i.e. include its term modulations in their assessment. In this work, the chosen approach consists of embedding its operation range through a polytopic description defined by its limits.

3.1. State-space formulation

Considering $\mathbf{x}(t) := [e(t)\ \dot{e}(t)]^T$, the impedance relationship (1) can be stated into continuous-time state-space form:

$$\dot{\mathbf{x}}(t) = \mathbf{A}^{\mathrm{c}}(t)\cdot\mathbf{x}(t) + \mathbf{B}^{\mathrm{c}}_F\cdot F(t), \tag{4}$$

where the force input matrix $\mathbf{B}_F$ and the state matrix $\mathbf{A}^{\mathrm{c}}$ are defined as

$$\mathbf{A}^{\mathrm{c}}(t) = \begin{bmatrix} 0 & 1 \\ -K(t)\cdot H^{-1} & -D\cdot H^{-1} \end{bmatrix}, \qquad \mathbf{B}^{\mathrm{c}}_F = \begin{bmatrix} 0 \\ H^{-1} \end{bmatrix}. \tag{5}$$

The product of state matrix $\mathbf{A}^{\mathrm{c}}(t)$ and $\mathbf{x}(t)$ can be further divided into a constant term $\mathbf{A}^{\mathrm{c}}_0$ and the control effort $u(t)$ corresponding to the VIC :

$$\mathbf{A}^{\mathrm{c}}(t)\cdot\mathbf{x}(t) = \mathbf{A}^{\mathrm{c}}_0\cdot\mathbf{x}(t) + \mathbf{B}^{\mathrm{c}}\cdot u(t) \tag{6}$$

where

$$\mathbf{A}^{\mathrm{c}}_0 = \begin{bmatrix} 0 & 1 \\ 0 & 0 \end{bmatrix}, \qquad \mathbf{B}^{\mathrm{c}} = \begin{bmatrix} 0 \\ 1 \end{bmatrix}, \qquad u(t) = \mathbf{W}(t)\cdot\mathbf{x}(t)\,;$$

where the variant VIC gain is:

$$\mathbf{W}(t) = \begin{bmatrix} -K(t)\cdot H^{-1} & -D\cdot H^{-1} \end{bmatrix}.$$

The nature of impedance relationship (1) renders (4) as a linear form with time dependency terms, namely Linear Time Variant (LTV).

3.2. LPV Model

If the variant terms of a LTV system can be arranged into a set of varying parameters $\Phi(t) = [\phi_1(t), ..., \phi_i(t), ..., \phi_{n_\phi}(t)]$, the system is referred as Linear Parameter Varying (LPV) Shamma (2012). In this work, the LPV form of (4) is obtained through the embedding of non-linear terms into $\phi_i(t)$, following Kwiatkowski et al. (2006). This approach constrains each scheduling variable (*i*) to be a-priori known, measured or estimated on-line and (*ii*) continuous and defined in the operation range. Hence:

$$\Phi(t) \equiv \phi_1(t) = -K(t)\cdot H^{-1}. \tag{7}$$

such that the LPV formulation is

$$\dot{\mathbf{x}}(t) = \mathbf{A}^{\mathrm{c}}(\Phi(t))\cdot\mathbf{x}(t) + \mathbf{B}^{\mathrm{c}}_F\cdot F(t), \tag{8}$$

where

$$\mathbf{A}^{\mathrm{c}}(\Phi(t)) = \begin{bmatrix} 0 & 1 \\ \phi_1(t) & -D\cdot H^{-1} \end{bmatrix}, \qquad \mathbf{W}^{\mathrm{c}}(\Phi(t)) = \begin{bmatrix} -\phi_1(t) & -D\cdot H^{-1} \end{bmatrix}. \tag{9}$$

Considering a non-zero H, variant stiffness $K(t)$ is (*i*) off-line determined from demonstrations given $K_{\max}$ and K_{min} through (2) and (*ii*) being defined from a linear operation over the covariance matrix of the H-GP model, is continuous and defined throughout time.

3.3. Polytopic representation

Properties can be assessed for LPV systems, but dealing with all their (infinite) reachable operating points defined by $\Phi(t)$ is not numerically tractable. Following Apkarian et al. (1995), if (*i*) $\Phi(t)$ ranges over a fixed polytope $\boldsymbol{\Theta}$ with n_v vertices $\boldsymbol{\theta}_i$, mathematically:

$$\Phi(t) \in \boldsymbol{\Theta} := \mathrm{Co}\{\boldsymbol{\theta}_1, ..., \boldsymbol{\theta}_i, ..., \boldsymbol{\theta}_{n_v}\}, \tag{10}$$

where n_v is the number of vertex and Co{} denotes that the polytope is defined as a convex hull, and (*ii*) system matrices dependence on $\phi_i(t)$ is

affine, then an LPV system can be defined by the polytope of system matrices evaluated at $\boldsymbol{\Theta}$, namely vertex systems. This is referred as a polytopic description, and allows to deal only with a set of vertex systems that are Linear Time Invariant (LTI). As these conditions are met for system (8), its polytopic definition is the following:

$$[\mathbf{A}^c(\Phi(t)),\ \mathbf{W}^c(\Phi(t))] \in \mathrm{Co}\left\{ [\mathbf{A}_i^c,\ \mathbf{W}_i^c] := [\mathbf{A}^c(\boldsymbol{\theta}_i),\ \mathbf{W}^c(\boldsymbol{\theta}_i)],\ i = 1, ..., n_v \right\}. \tag{11}$$

To define $\boldsymbol{\theta}_i$, in this work, the *bounding box* method Sun and Postlethwaite (1998) is applied such that each vertex is the combination of lower and upper bounds of each varying parameter $\underline{\phi_i}$ and $\overline{\phi_i}$, which leads to $n_v = 2^{n_\phi}$ and sets that $\boldsymbol{\theta}_i \in \mathbb{R}^{n_\phi}$. For the VIC case, these limits can be obtained through the evaluation of (7) throughout the extracted stiffness profile from (2) for the complete execution.

Hence, using the polytopic description each $\mathscr{C}_s$ can be linked to a set of vertex systems to be used in the forthcoming assessment of conditions. Figure 2 summarises the complete process in the context of this work. It is important to note that definitions (11) are for the continuous-time form of the system. As aforementioned, to acknowledge the real execution on robotic platforms, controller assessment conditions are stated for discrete implementations. Following Toth et al. (2010), their discrete-time equivalents are obtained by evaluating system's matrices according to a discretisation method with a sampling time T_s. Details on the particular application to the platform used in work are included in Sect. 6.

4. VIC Solution Assessment

The method proposed in this work aims at finding controller solutions $\mathscr{C}_s$ that define a VIC fulfilling a set of conditions. Hence, they are stated into an assessment problem of $\mathscr{C}_s$, differentiating between conditions regarding safety and performance. Safety ones bound controller operation by limiting a region within the $\mathscr{C}_s$ space. On the other hand, performance conditions define criteria that determine VIC suitability for the task within the $\mathscr{C}_s$ space. Thus, the complete assessment is used to find solutions at the intersection of both, i.e. those suitable for the task with a bounded operation. Moreover, some of these conditions can be formulated as constraints over the complete operation range of the VIC thanks to its polytopic representation. Thus, these constraints can be stated in the form of Linear Matrix Inequalities (LMIs) to each of the vertex system, such that, if a common solution is found, the constraint is fulfilled for the complete operation range. With respect to our previous work San-Miguel et al. (2022), additional safety conditions in the form of LMIs are included, and performance condition is not embedded as an LMI constraint but corresponds to an heuristic that introduces user intuition over the required compliant behaviour.

4.1. Safety

As aforementioned, the paramount concern when designing a controller is to preserve stability, which can be formulated as a constraint in the form of LMIs.

Proposition 1. *Stability LMI Constraints for VIC. Considering the discrete form of the polytopic description (11) for LPV model (8), the equilibrium* $\mathbf{x} = \mathbf{0}$ *is stable in the sense of Lyapunov for* $k = [0, \infty) \in \mathbb{N}$ *if there exist a solution matrix* $\mathbf{P} > \mathbf{0} \,|\, \mathbf{P} = \mathbf{P}^T$ *that simultaneously fulfils the following LMI* $\forall i = 1, ..., n_v$*:*

$$\mathbf{A}_i^T \cdot \mathbf{P} \cdot \mathbf{A}_i - \mathbf{P} \leq \mathbf{0} \tag{12}$$

Proof: The proof is given in App. A.1.

Besides stability, it is desirable to set limits over variables that define controller behaviour. This allows to set guarantees over task execution beforehand. For VIC, upper bounds for position error $\Delta p_{\max}$ and control effort $u_{\max}$ can be simultaneously introduced using LMI constraints.

Proposition 2. *Maximum Effort and Error LMI Constraints for VIC. Considering the discrete form of the polytopic description (11) for LPV model (8), conditions*

$$u(k) \leq u_{\max}\,, \qquad |e(k)| \leq \Delta p_{\max}\,; \tag{13a,b}$$

are satisfied for $k = [0, \infty) \in \mathbb{N}$ *and an initial state* $\mathbf{x}(0)$ *if there exist a solution matrix* $\mathbf{P} > \mathbf{0} \,|\, \mathbf{P} = \mathbf{P}^T$ *that simultaneously fulfils the following LMI* $\forall i = 1, ..., n_v$*,*

$$\begin{bmatrix} u_{\max}^2 & \mathbf{W}_i \\ \mathbf{W}_i^T & \mathbf{P} \end{bmatrix} \geq \mathbf{0}\,, \qquad \begin{bmatrix} \mathbf{P} & \mathbf{A}_i^T \cdot \mathbf{S}^T \\ \mathbf{S} \cdot \mathbf{A}_i & \Delta p_{\max}^2 \end{bmatrix} \geq \mathbf{0}\,; \tag{14a,b}$$

where $\mathbf{S}$ *is a selection matrix for* $e(k)$*; and such that*

$$\begin{bmatrix} 1 & \mathbf{x}(0)^T \cdot \mathbf{P} \\ \mathbf{P} \cdot \mathbf{x}(0) & \mathbf{P} \end{bmatrix} \geq \mathbf{0}\,; \tag{15}$$

where $\mathbf{I}_0$ *a matrix of the appropriate dimensions.* *Proof:* The proof is given in App. A.2.

Another relevant characteristic defining control behaviour is the transient response of the system, i.e. how it behaves until reaching the steady state. In second-order systems like (1) exponentially decaying oscillations might appear. This phenomenon is associated to damping ratio $\boldsymbol{\xi} \in (0, 1)$, i.e. underdamped systems. This can be characterised through the Percentage Overshooting (*OS*), which corresponds to the maximum peak value of the system measured from the reference, and can be expressed as function of $\boldsymbol{\xi}$. Hence, in this work, vertex systems' poles are confined into a region in the discrete complex plane which imposes a maximum damping ratio $\overline{\boldsymbol{\xi}}$ that corresponds to a maximum Percentage Overshooting $\overline{OS}$. This is defined through LMI constraints based on the concept of $\mathbb{D}$-stability.

Proposition 3. *Maximum Overshooting LMI Constraints for VIC. Considering the discrete form of the polytopic description (11) for LPV model (8), system's response will not surpass the maximum percentage overshoot* $\overline{OS}$ *if there exist a solution matrix* $\mathbf{P} > \mathbf{0} \,|\, \mathbf{P} = \mathbf{P}^T$ *that simultaneously fulfils the following LMI* $\forall i = 1, ..., n_v$*:*

$$\boldsymbol{\alpha} \otimes \mathbf{P} + \boldsymbol{\beta} \otimes (\mathbf{P} \cdot \mathbf{A}_i) + \boldsymbol{\beta}^T \otimes \left(\mathbf{A}_i^T \cdot \mathbf{P}\right) \leq \mathbf{0} \tag{16}$$

being $\boldsymbol{\alpha} = \mathrm{diag}(\boldsymbol{\alpha}_e,\ \boldsymbol{\alpha}_v)$, $\boldsymbol{\beta} = \mathrm{diag}(\boldsymbol{\beta}_e,\ \boldsymbol{\beta}_v)$ *defined according to Rosinová and Hypiusová (2019) as follows:*

$$\boldsymbol{\alpha}_e = \begin{bmatrix} -1 & -\dfrac{a_{se}}{a_e} \\ * & -1 \end{bmatrix}, \quad \boldsymbol{\beta}_e = \frac{1}{2} \begin{bmatrix} 0 & \dfrac{1}{a_e} - \dfrac{1}{b_e} \\ \dfrac{1}{a_e} + \dfrac{1}{b_e} & 0 \end{bmatrix}; \tag{17a,b}$$

$$\boldsymbol{\alpha}_v = -2 \cdot [\sin(\gamma) \quad 0* \quad \sin(\gamma)], \quad \boldsymbol{\beta}_v = \begin{bmatrix} \sin(\gamma) & \cos(\gamma) \\ -\cos(\gamma) & \sin(\gamma) \end{bmatrix}; \tag{17c,d}$$

where

$$\overline{\boldsymbol{\xi}} = -\log(\overline{OS}/100) \Big/ \sqrt{[b]\pi^2 + \log^2(\overline{OS}/100)}\,; \tag{18a}$$

$$\varphi = \cos^{-1}(\overline{\boldsymbol{\xi}})\,; \qquad a_0 = -e^{-\pi/\tan\varphi}\,; \tag{18b,c}$$

$$a_{se} = (1 + a_0)/2, \qquad a_e = (1 - a_0)/2\,; \tag{18d,e}$$

$$b_e = b \cdot a_e \Big/ \sqrt{[b]a_e^2 - (a - a_{se})^2}\,; \tag{18f}$$

$$\gamma = \tan^{-1}(b/(1 - a)). \tag{18g}$$

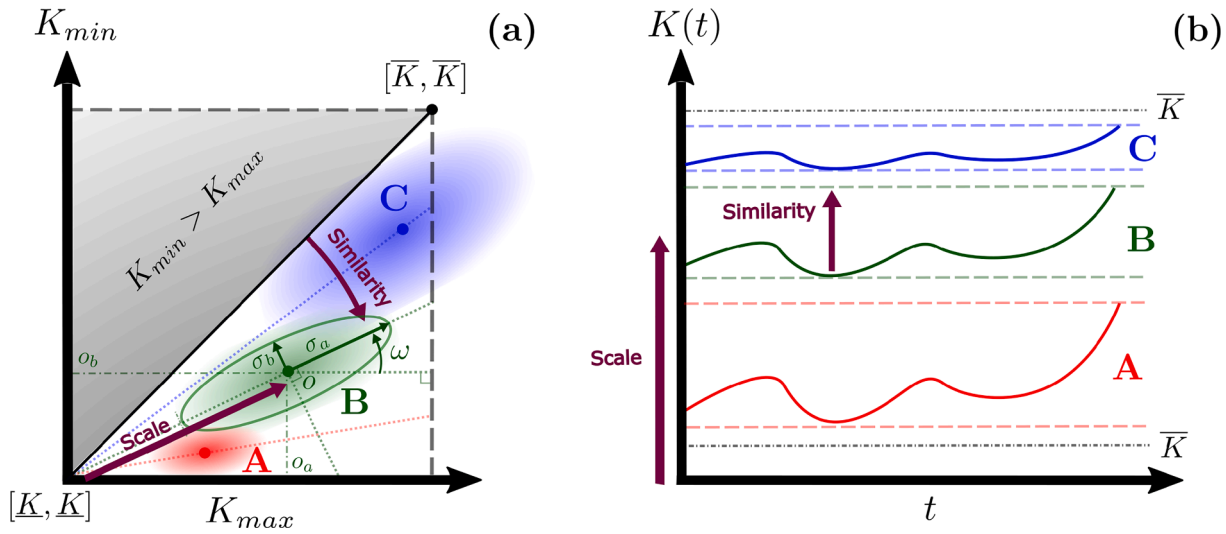

Fig. 3. Graphical representation of the User Preference mechanism for three different cases on the same compliance profile in $K_{\max} - K_{\min}$ plane (a) and the corresponding K profiles (b). Case A has both low Scale and Similarity values, which translates into a stiffness modulation $K(t)$ with a $K_{\min}$ closer to $\underline{K}$ and very distinct from $K_{\max}$. For B, both $K_{\min}$ and $K_{\max}$ have higher values than in A as the Scale is higher, but also a higher Similarity makes their values closer. Case C has both high Scale and Similarity values and therefore both $K_{\min}$ and $K_{\max}$ are closer to $\overline{K}$ with similar values.

where $\mathrm{Re}(\mathbf{r}) = a$ *and* $\mathrm{Im}(\mathbf{r}) = b$*, where* $\mathbf{r}$ *is a point in the complex discrete plane belonging to the logarithmic spiral defined by* φ*.*

Proof: The proof is given in App. A.3.

4.2. Performance

In many cases, how successfully a task is performed by a robot depends on how well human intuition is introduced into its execution. The LfD technique described in Sect. 2 only allows to specify the compliance profile through a set of demonstrations on the same task, but the user has no means to introduce the desired rigidity associated with each maximum and minimum level of compliance. Therefore, performance is assessed through an heuristic that characterises desired compliance along the task, namely User Preference. Particularly, it is defined in the controller solution plane region described by the maximum $\overline{K}$ and minimum $\underline{K}$ values of K_{max} and K_{min} through two parameters ranging in [0,1]: Similarity and Scale. Similarity defines the "closeness" between K_{max} and K_{min}, and Scale where the profile remains within $\left[\underline{K}, \overline{K}\right]$. Thus, User Preference heuristic provides a "distance" of $\mathscr{C}_s$, particularly of $K^s_{\max}$ and $K^s_{\min}$, to a desired $\mathscr{C}^d_s$ with $K^d_{\max} \equiv o_a$ and $K^d_{\min} \equiv o_b$ described through Scale and Similarity. Mathematically it is defined as an elliptical Gaussian function:

$$\omega = \mathrm{Sim}\cdot\pi/4\,; \tag{20a}$$

$$o_a = \mathrm{Scale}\cdot\left(\overline{K} - \underline{K}\right) + \underline{K}\,; \qquad o_b = o_a\cdot\tan\omega + \underline{K}\,; \tag{20b,c}$$

$$\sigma_a = \frac{o_a - \underline{K}}{2\cos\omega}\,; \qquad \sigma_b = \frac{o_b - \underline{K}}{\cos\omega}\,; \tag{20d,e}$$

Thus, in the $K_{\max} - K_{\min}$ plane, Similarity determines the angle between diagonal $K_{\max} = K_{\min}$ and the direction of the major axis of the elliptical Gaussian function through $\left(\underline{K}, \underline{K}\right)$. This defines the angle ω of its major axis w.r.t. $K_{\max}$ axis according to Eq. (20a a). Thus, according to the constraint $K_{\min} > K_{\max}$ from Eq. (1), null Similarity corresponds to $\omega = 0$ rad and Similarity equal to 1 corresponds to $\omega = \pi/4$ rad. Equations (20a b,c) define the centre of the elliptical Gaussian function $o = (o_a, o_b)$ according to Scale, considering the projection of allowed stiffness range $\left[\underline{K}, \overline{K}\right]$ on it. For example, Scale equal to 0.5 will set the centre of the elliptical Gaussian function in $K_{\max}$ at the middle value in $\left[\underline{K}, \overline{K}\right]$, and in $K_{\min}$ at half the projection of $\left[\underline{K}, \underline{K}\right]$ according to ω. Standard deviations in major and minor axis σ_a and σ_b, respectively, are defined in Eqs. (20a d,e) in terms of the distances of o w.r.t. limits of $K_{\max} - K_{\min}$ plane along its axes. Figure 3 includes a graphical representation of the User Preference heuristic for three different Similarity and Scale configurations on the same compliance profile.

Note that desired compliance can also be rendered through other techniques such as the definition of Q and R in an LQR criterion as in our previous work San-Miguel et al. (2022). But, under out point of view, User Preference relates better to compliant behaviour as it shapes a term within the impedance relationship so the effects of its parameters can be

$$\text{U.Pref.}(\mathscr{C}_s,\ \text{Scale},\ \text{Sim.}) := \exp\left(\begin{bmatrix} K^s_{\max} - o_a \\ K^s_{\min} - o_b \end{bmatrix}^T \cdot \boldsymbol{\Sigma}_{\text{U.Pref.}}(\text{Scale},\ \text{Sim.}) \cdot \begin{bmatrix} K^s_{\max} - o_a \\ K^s_{\min} - o_b \end{bmatrix}\right) \tag{19}$$

where

$$\boldsymbol{\Sigma}_{\text{U.Pref.}}(\text{Scale},\ \text{Sim.}) = -\begin{bmatrix} \frac{\cos^2\omega}{2\sigma_a^2} + \frac{\sin^2\omega}{2\sigma_b^2} & -\frac{\sin 2\omega}{4\sigma_a^2} + \frac{\sin 2\omega}{4\sigma_b^2} \\ -\frac{\sin 2\omega}{4\sigma_a^2} + \frac{\sin 2\omega}{4\sigma_b^2} & \frac{\sin^2\omega}{2\sigma_a^2} + \frac{\cos^2\omega}{2\sigma_b^2} \end{bmatrix}$$

such that

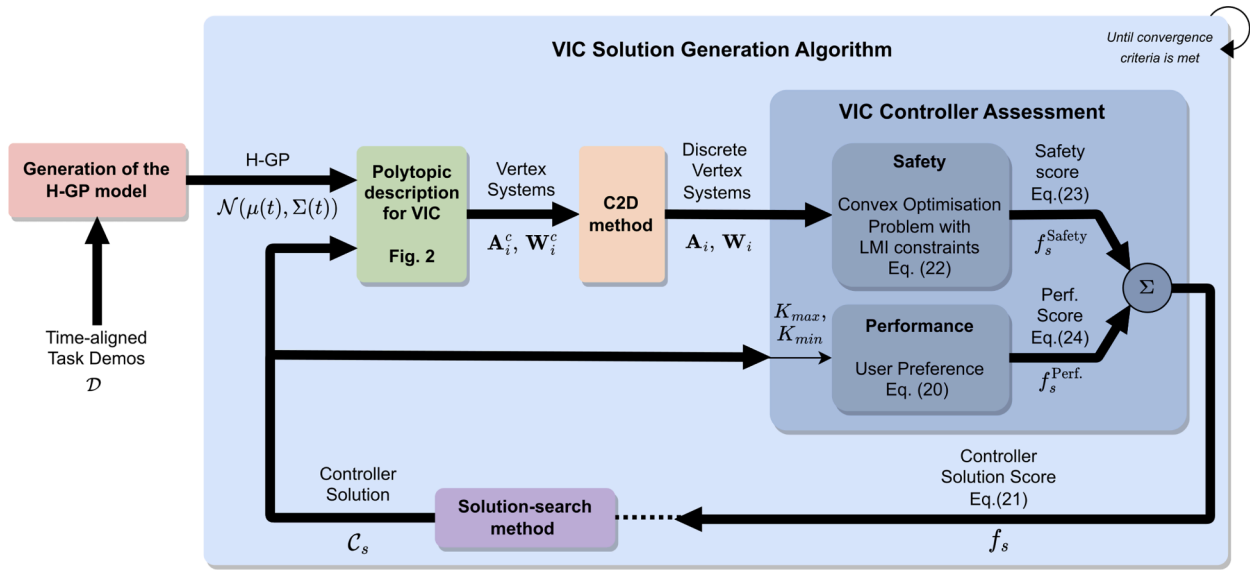

Fig. 4. Complete scheme of the automated generation of controller solutions for LfD-based VIC description, based on proposed condition assessment.

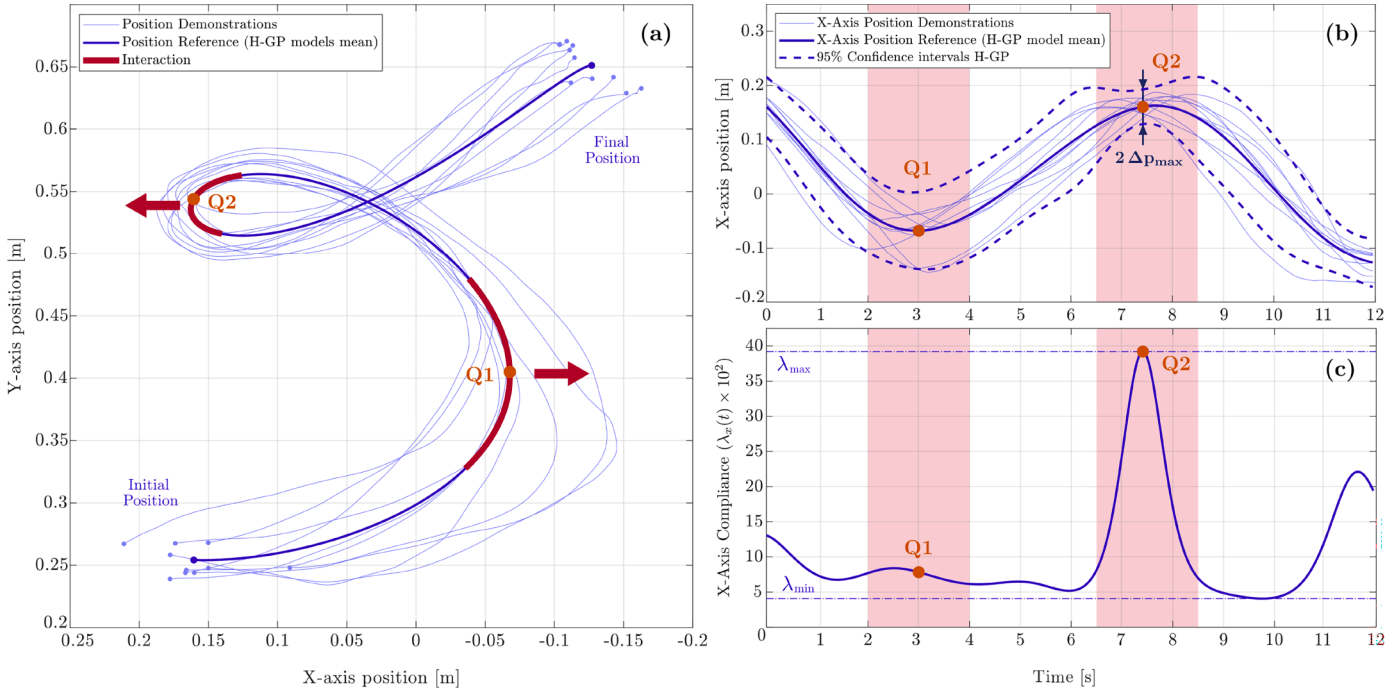

Fig. 5. Demonstrations of the validation trajectory and generated reference trajectory (a) together with the H-GP mean and confidence intervals for the X axis (b) and the corresponding compliance profile (c). Regions where a constant virtual force of 50 N is applied in opposite directions are highlighted in the reference trajectory in (a) and represented as shadowed areas in (b) and (c), together with the points Q1 and Q2 where compliancy is evaluated.

easily understood by non-expert user. On the other hand, LQR relates to the overall behaviour of the system as there not exist a direct relationship between particular Q and R values and a certain desired compliant behaviour. Moreover, User Preference is defined according to the allowed range of values for $K(t)$ such that it generalises to different platforms or scenarios. With an LQR condition alone, this can not be impose this through Q and R.

5. Automated VIC Solution Generation

Controller solution assessment as presented in the previous Section only regards about determining whether the tuple of parameters that describes the VIC fulfils a set of conditions or not. As the method seeks one controller solution to be used in the VIC, condition assessment needs to be formulated in order to provide a score that determines the overall suitability of the solution. Hence, in this work, for each controller solution $\mathscr{C}_s$, a compound suitability score f_s is obtained as the sum of its safety and performance scores:

$$f_s = f_s^{\text{Safety}} + f_s^{\text{Perf.}}. \tag{21}$$

Considering the definition of safety conditions given in this work, its corresponding score needs to characterise the narrower allowable region in the controller solution space, i.e. how much *safer* is $\mathscr{C}_s$ among all the solutions. Hence, making use of the convexity property of LMIs, safety

Table 1
Constant impedance controller gains for KINOVA GEN3 manipulator. Considering it imposes a 2nd-order dynamic behaviour, D is computed as a function of K and H with a damping ratio of 0.8.

DoF Type	H	K	D
Translational	2 kg	10000 N/m	$2{\cdot}0.8\sqrt{K{\cdot}H}$ N·s
Rotational	1 kg · m^2	1500 N·m	$2{\cdot}0.8\sqrt{K{\cdot}H}$ N·s ·m

conditions are stated into a convex optimisation problem for the polytopic description of the system obtained from $\mathscr{C}_s$ (Fig. 2) to minimise squared limit control effort $u^2_{\max}$ (with a maximum value $\overline{u_{\max}}^2$) as follows [1]:

$$\begin{array}{ll} \text{For} & \mathbf{A}_i\,, \mathbf{W}_i \quad \forall i = 1, ..., n_v \\ \text{find} & \mathbf{P} \\ \text{minimising} & u^2_{\max} \\ \text{subject to} & (12),\ (14\text{a, b}),\ (15),\ (16) \\ \text{given} & \mathbf{x}(0),\ \Delta p_{\max},\ \overline{OS}, \end{array} \tag{22}$$

such that

$$f_s^{\text{Safety}} = u_{\max} / \overline{u_{\max}}. \tag{23}$$

Therefore, the only values to be *a-priori* defined for controller assessment are a maximum control effort limit $\overline{u_{max}}$, and $\mathbf{x}(0)$, Δp_{max}, and $\overline{OS}$ for the problem stated in (22). How these values are assigned is addressed in Sect. 6. Performance score is derived from User Preference heuristic (19), according to desired Scale and Similarity:

$$f_s^{\text{Perf.}} = 1 - \text{U.Pref.}(\mathscr{C}_s,\ \text{Scale},\ \text{Sim.}). \tag{24}$$

Hence, the complete solution generation scheme is designed to obtain the most suitable one $\mathscr{C}_s^*$ with the minimal score f_s^*, i.e. the f_s closest to desired Similarity and Scale that fulfils the safety constraints with the minimum control effort. First, the solution-search method iteratively provides controller solution candidates $\mathscr{C}_s$ within the limits given to each parameter. Additionally, to obtain the desired behaviour by the LfD technique described in (2), constraint $K_{\max} > K_{min}$ is imposed at this step. Then, its polytopic description is obtained as described in Sect. 3, considering the H-GP model that embeds task demonstrations. The discrete-time form of vertex systems are used for LMI constraints on the problem regarding safety conditions assessment stated in (22) to obtain f_s^{Safety}. Simultaneously, performance is assessed directly on $\mathscr{C}_s$ providing $f_s^{\text{Perf.}}$. Together they compound the suitability score f_s, which is provided to the solution-search method to generate next candidates towards the most suitable one until the convergence criteria is met, i.e. $\mathscr{C}_s \approx \mathscr{C}_s^*$. Figure 4 graphically depicts the complete process.

6. Validation Experiments

The method presented in this paper is validated on a trajectory tracking task using a KINOVAGEN3 robotic manipulator [2]. As in some validation experiments it is not possible to ensure a safe execution of the task beforehand, task execution has been carried out in the physic-based simulator SIMSCAPE MULTIBODYwithin the MATLABprogramming ecosystem. As in the real platform, implemented control strategy renders (1) through the well-known inverse dynamic approach to compensate for non-linear effects, also replicating its discrete-time execution.

The task trajectory corresponds to a planar (2-DoF) "wiping" movement along a surface, which is embedded in H-GP models (one per axis) using a set of 10 user-guided demonstrations as shown in Fig. 5a, obtained according to the details provided in App. B.1. Notice that initial positions for demonstrations are randomly generated (within a given interval) in order to avoid null variability (and consequently highest stiffness value) at the beginning of the task. To better analyse the behaviour of different controller solutions, VIC is applied only for X-axis control, while (constant) IC described in Table 1 are used for remaining DoFs. From the H-GP covariance, represented in Fig. 7b by the 95% confidence intervals, the compliance profile determined by $\lambda(t)$ is obtained (Fig. 7c). Based on it, to evaluate compliant behaviour along the task, a constant force is virtually introduced during trajectory execution twice: in a high compliance (low stiffness) region between 2 and 4 s and in a low compliance (high stiffness) region between 6.2 and 8.2 s. In each of these regions, the compliant behaviours will be evaluated at certain point, namely Q1 and Q2. Force magnitude is equal in both cases but it is first applied in the negative axis direction and then in the opposite one.

Prior to the generation of VIC solutions, the different parts that compound the method must be defined according to the task and platform. First, given parameters to the optimisation problem (22) have to be determined. Initial state $\mathbf{x}(0)$ is obtained from the reference trajectory generated by H-GP models, considering that the robot starts at the initial point of the reference trajectory with null velocity. Remaining parameters are assigned by the user, in this case $\Delta p_{\max}$ is considered to be the minimum difference between the 95% confidence bounds and reference trajectory from the H-GP model(Fig. 5b), having a value of 3.19 cm. Considering experience on the real platform, $\overline{u_{\max}} = 10$ N/kg and $\overline{PO} = 5\%$. For the solution-search method, bounds on $\mathscr{C}_s$ parameters are given to avoid noise amplification effects on the real platform such that K_{min} and $K_{\max}$ have been limited to [0,10000] N/m and D to [0,2500] N·s/m. The VIC description is completed with $H = 2$ kg, determined according to robot hardware Dietrich et al. (2021). The discretisation process of vertex systems' matrices is performed considering signal processing on the platform, hence using Zero-order hold with a sampling time $T_s = 1{\cdot}10^{-3}$ s (as control-loop frequency is 1 kHz).

Controller solutions are obtained for four sets of User Preferences describing different behaviours, labeled as I-IV. For each one, four designs have been performed to analyse the effect of introducing each LMI constraint into the optimisation problem (22). Thus, Design A has no constraints (only considers User Preference), Design B incorporates stability constraint (12), Design C adds the limitations on position error and control effort (14a,b), and finally Design D incorporates the maximum overshooting constraint, i.e. the complete optimisation problem as stated in (22) [3]. Additionally, to evaluate the effect of solution-search method convergence, for each User Preference - Design combination, 10 solution controllers have been obtained under different initial settings of the method. Only those controller solutions with $f_s^{\text{Perf.}}$ closest to the mean value of all the generated ones are chosen for task execution. Under the implementation detailed in App. Appendix B solutions depicted in Figure 6 at the controller parameter space are obtained, and Table 2 summarises the details of chosen ones for execution. These results can be replicated using the demo version of the complete method available in the project webpage [4]Project webpage: http://www.iri.upc.edu/groups/perception/#LMI_VIC_LfD..

[1] For the implementation of the optimisation problem, the minimisation of u_{max} makes it non-convex due to constraint (14a,b a). Therefore, u^2_{max} is used as the minimisation objective instead, as it implies the minimisation of u_{max}.

[2] GEN3 robotic manipulators by KINOVAhttps://www.kinovarobotics.com/product/gen3-robots

[3] As Designs A and B do not incorporate LMI constraints with u^2, the norm of solution matrix $\mathbf{P}$ is internally used as minimisation objective, but is not assigned to f_s^{Safety}.

[4] ProjectWeb

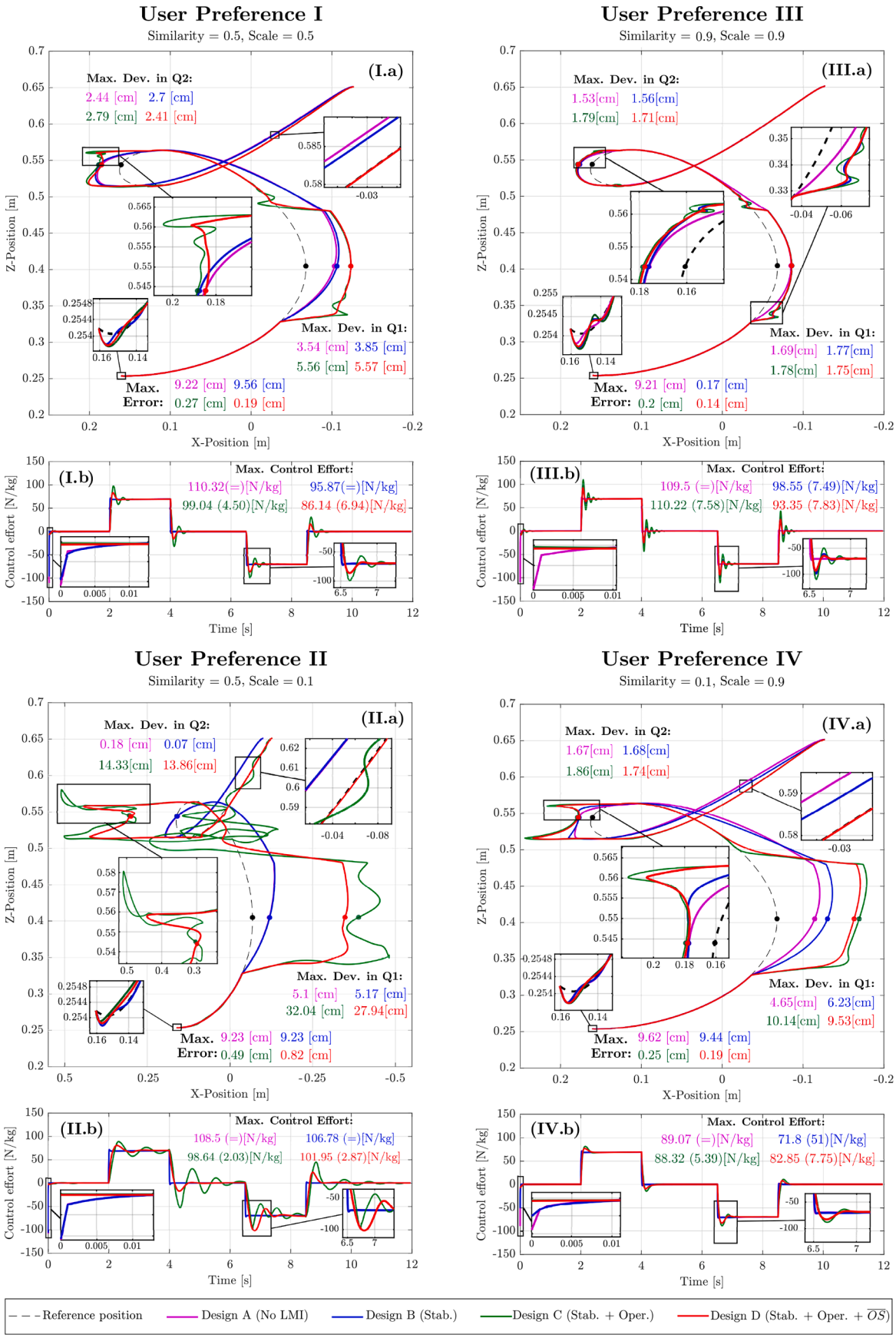

Fig. 7. Validation trajectory execution and control effort evolution using the VIC solution of each User Preference - Design combination. For User Preference N, Figure N.a represents the end-effector position together with the maximum absolute trajectory error at the beginning of the task and deviations at Q1 and Q2, and Figure N.b depicts the evolution of the control effort and its maximum absolute values along the task and before force application (in parenthesis) annotated.

Table 2
Controller solutions for each User Preference - LMI Design combination, together with their corresponding value of User Preference score (f_S^{User}) and limit control effort ($u_{\max}$).

Design	$f_s^{\text{Perf.}}$	$u_{\max}$ N/kg	$K_{\max}$ N/m	$K_{\min}$ N/m	D N·s/m
A	7.81×10^{-5}	-	4999	2086	2497
B	6.68×10^{-3}	-	4940	2067	2169
C	3.8×10^{-3}	4.61	5019	2181	71
D	7.24×10^{-2}	6.94	4803	1987	157
(a) User Preference I: Similarity = 0.5, Scale = 0.5					
Design	$f_s^{\text{Perf.}}$	$u_{\max}$ N/kg	$K_{\max}$ N/m	$K_{\min}$ N/m	D N·s/m
A	9.02×10^{-4}	-	990	402	2455
B	1.43×10^{-4}	-	997	409	2416
C	3.13×10^{-2}	2.23	902	343	17
D	4.08×10^{-3}	2.87	988	431	65
(b) User Preference II: Similarity = 0.5, Scale = 0.1					
Design	$f_s^{\text{Perf.}}$	$u_{\max}$ N/kg	$K_{\max}$ N/m	$K_{\min}$ N/m	D N·s/m
A	1.12×10^{-5}	-	9018	7671	2478
B	3.27×10^{-6}	-	8986	7687	139
C	2.35×10^{-2}	7.58	7814	7759	74
D	1.21×10^{-2}	7.83	8181	7847	177
(c) User Preference III: Similarity = 0.9, Scale = 0.9					
Design	$f_s^{\text{Perf.}}$	$u_{\max}$ N/kg	$K_{\max}$ N/m	$K_{\min}$ N/m	D N·s/m
A	5.66×10^{-5}	-	8961	703	2016
B	1.92×10^{-3}	-	9261	721	1154
C	5.68×10^{-2}	5.55	7467	599	122
D	2.47×10^{-2}	7.75	8002	621	175
(d) User Preference IV: Similarity = 0.1, Scale = 0.9					

6.1. Results

Figure 7 shows trajectory executions of the controller solutions obtained for each User Preference - Design combination under the introduction of virtual forces. User Preference I sets a desired compliant behaviour centered in both Scale and Similarity ranges. Both controllers generated from Designs A and B present a highly damped behaviour along the task with respect to Designs C and D, due to the high values of D gain. Those designs do not include LMI constraints able to fix its value, and, for that reason, the solution generation method randomly assigns it within the allowed range, which can be seen in Fig. 6.I.b. As Fig. 7.I.a shows, this produces a "slow" reaction when force is applied, which is most noticeable in the first region, where the robot is driven gradually away from the trajectory. This also affects the behaviour when force disappears, maintaining a high position tracking error for longer than solutions from Designs C and D. Regarding control effort (Fig. 7.I.b) this leads to an unbounded value that takes its highest value (considering the no-force sections of the trajectory) at the initial point. It should be mentioned that having a non-zero control effort at the beginning of the task is a consequence of the procedure to obtain the reference velocity from the position mean of the H-GP model, which generates an initial non-zero velocity reference. Therefore, as the robot starts stalled, a control effort is generated to reach reference velocity. This does not happen with Designs C and D as they introduce a condition that provides an upper bound of the control effort (again, under no external force) considering $\mathbf{x}(0)$. Between these two designs, the most recognisable difference is the tracking behaviour (Fig. 7.I.a) when the force is applied and fades out: while the controller from Design C presents a noticeable oscillatory response, the one from Design D presents a softened reaction, which becomes more noticeable at the beginning of second force application. This is an effect of minimising the maximum control effort, leading to low values of D that still fulfil the maximum deviation condition. By introducing the maximum overshooting condition in Design D, although the maximum control effort is minimised, D is set to a higher value in order to reduce the oscillatory behaviour. This can also be observed for the control effort evolution in Fig. 6.I.b. Note that in both Designs C and D control effort evolution present lower values at the beginning (fulfilling the bounds defined by design in Table 2 a), obtaining the lowest one with Design D solution. Also the max. error (evaluated before first force applications) remains below the value of $\Delta p_{\max}$ chosen from the H-GP model in both designs.

Similar conclusions can be drawn for the remaining User Preferences with some particularities on each case. From User Preference I to II Scale is reduced to 0.1 while Similarity is maintained at 0.5. This generates solutions closer to the lower limits of the stiffness domain with Similarity again centered in the interval. Thus, high and low compliance

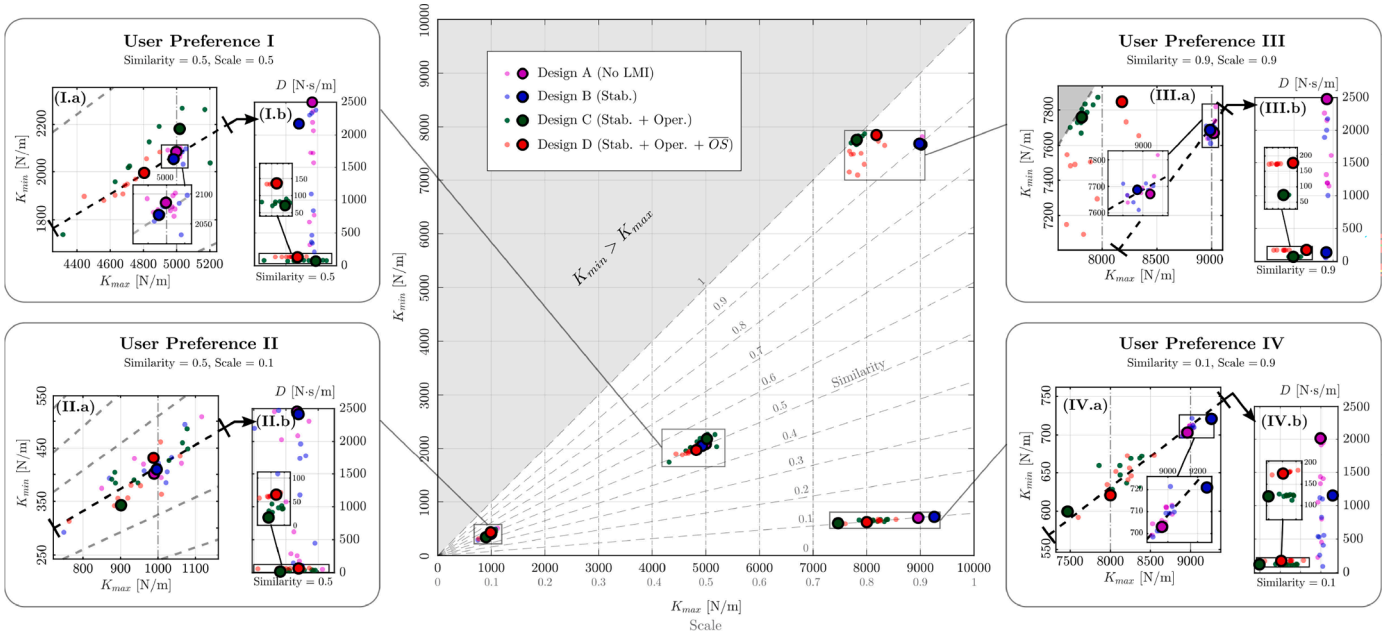

Fig. 6. Controller solution space with the ones generated for each User Preference - Design combination. Central figure represents stiffness plane ($K_{\max} - K_{\min}$) and, for User Preference N, Figure N.a represents a zoom over the region with all the obtained solutions. Figure N.b represents the (vertical) projection over the corresponding Similarity plane to visualize D values. Chosen controller solutions are represented by larger size dots.

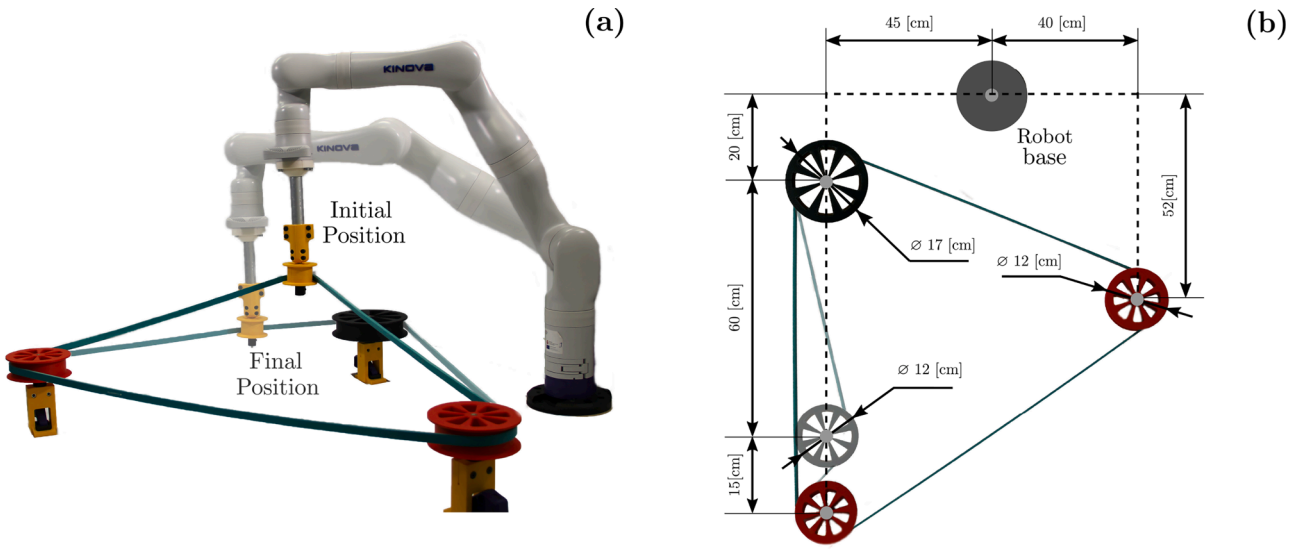

Fig. 8. Belt Drive unit setup for Case Study. Figure a depicts the initial and final (shadowed) positions of the KINOVA manipulator and belt configurations. Figure b includes the distribution of the pulleys w.r.t. the robot base, including the idler pulley (shadowed) for the first one-off modification scenario.

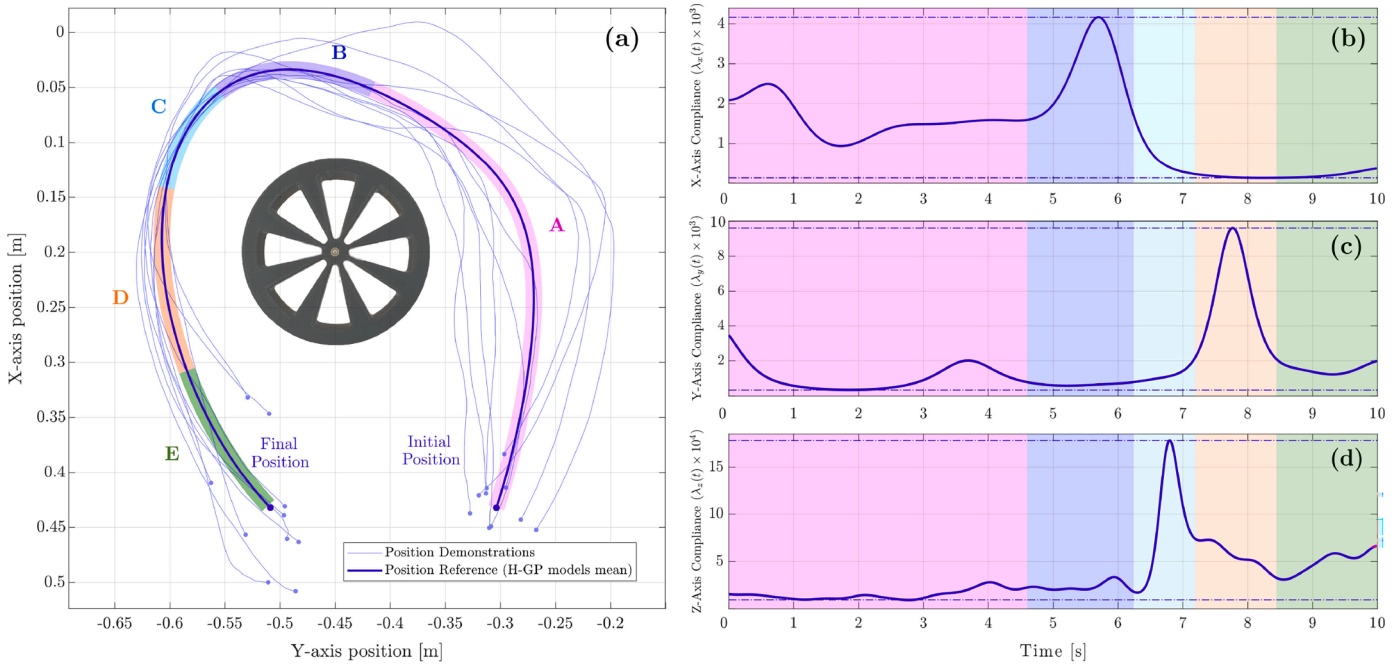

Fig. 9. Demonstrations of the looping task trajectory and generated reference trajectory (a) together with the corresponding compliance profiles in *X* (b), *Y* (c) and *Z* (d)-axes. The different task regions are highlighted in the reference trajectory in (a) and represented as shadowed areas in (b-d). Region A corresponds to the approach movement from the initial position to the pulley (low/medium stiffness in all three axis), Regions B to D to the stiffness maximum in *X* (beginning of the looping action), *Z* (to ensure downwards movement is performed to engage belt) and *Y*-axes (to avoid colliding the pulley), respectively. Region D is for the last movement away from the pulley to the final position.

behaviours are quite similar but still maintain a substantial contrast, represented by the maximum deviations in Q1 and Q2. Regarding the differences between designs, controllers from A, B and D present similar characteristics than the ones obtained for User Preference I. For C, a lower *D* together with the low values of K_{min} and K_{max} due to Scale causes an erratic behaviour on the second force application, as it can be observed in Fig. 7.II.b. For User Preference III, both Similarity and Scale are increased to 0.9, which translates into high and similar values for K_{max} and K_{min}. Thus, the difference between maximum deviations under different compliance levels for this case is the smallest (between 0.01 and 0.14 cm). In this case, all the controllers behave similarly for the tracking task (Fig. 7.III.a) but there exist still differences during force application, being the reaction from Design D controller faster than A but with less oscillations than D. Notice that in this case, controller obtained with Design B has almost the same behaviour as the one from Design D, due to their similar *D* gain. Again, as with Design A, this gain is not fixed by any constraint and its value is randomly assigned (Fig. 7.III. b). Finally, from User Preference III to IV only Similarity is changed to 0.1, which generates a variant controller solution that presents the greatest deviations differences between Q2 and Q1 from 3 to almost 9 cm. As in User Preference I, Designs A and B do present a damped tracking behaviour (Fig. 7.IV.a) that slows its response under force application, leading to high trajectory tracking errors. In this case, controllers from both Designs C and D have a quite similar response

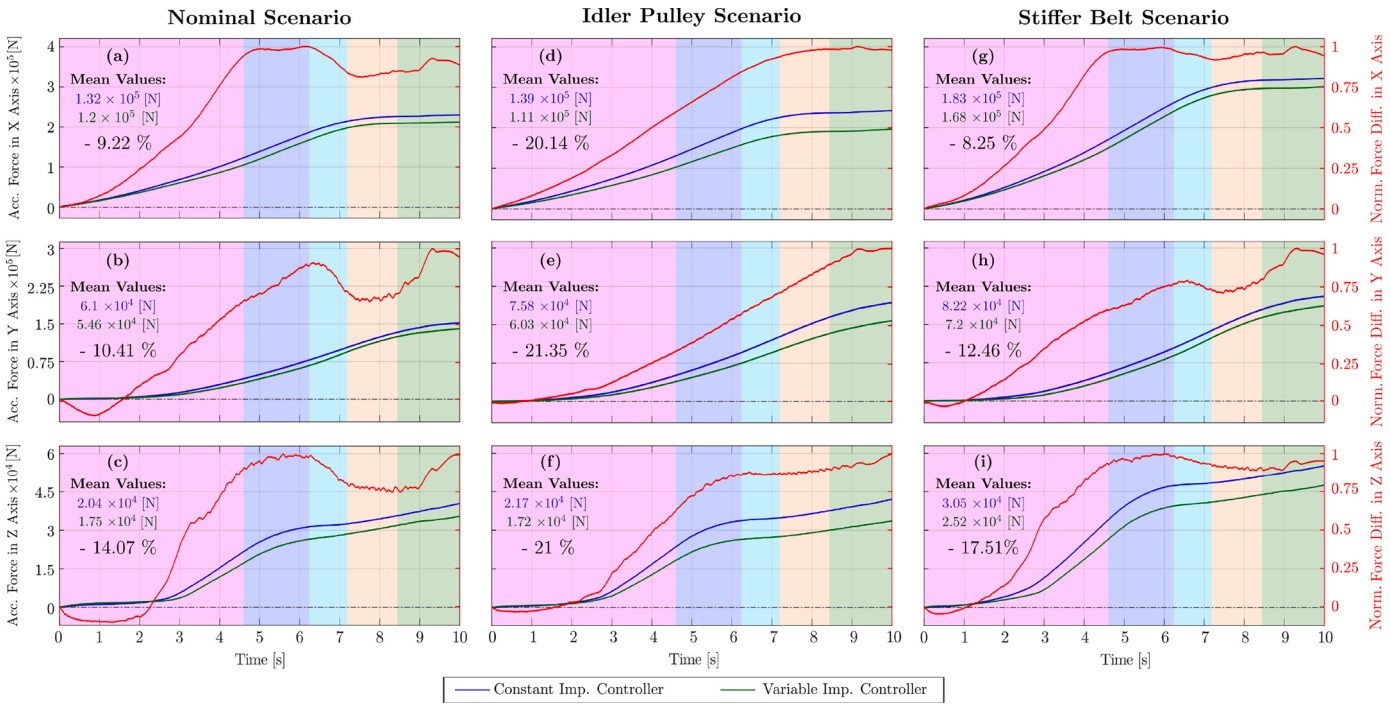

Fig. 10. Accumulated Force of the Constant and Variable Impedance Controller solutions together with the Normalized Difference (w.r.t. the maximum value) between them for X, Y and Z axis on the three scenarios for the Belt Unit Case Study: Nominal (a-c), Idler Pulley (d-f) and Stiffer Belt (g-i). For each one, the mean accumulated force values and the reduction/increase that the value for the variable controller represents over the constant one have been also included.

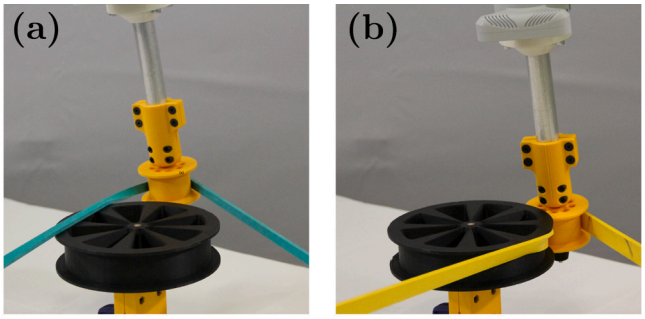

Fig. 11. Task execution errors on the Belt Unit using the nominal controller solutions (Table 3 a) on the Idler Pulley (a) and Stiffer Belt (b) scenarios.

although an oscillatory behaviour is still present in the former one, being most noticeable at the beginning of the first force application. Finally note that both max. control effort (Tables 2 a - 2 d) and max. deviation bounds are fulfilled by Designs C and D for all User Preferences.

All trajectory executions are summarised into a video provided as supplementary material and also available in the project webpage[4].

7. Case Study

Finally, the method proposed in this work is evaluated on a real case study. Following the Assembly Challenge on the Industrial Robotics Category in World Robot Summit 2018 Yokokohji et al. (2019), the task consists on looping a belt over the last pulley in a belt drive unit (Fig. 8). Within the Challenge, this task aimed at evaluating the manipulation of flexible objects on a complex trajectory while interacting with other elements. Hence, the method presented in this work is used to provide a task definition through demonstrations such that a VIC is generated to reduce stress over the belt during execution w.r.t. a constant rigid controller. Moreover, as in the Challenge, slight one-off modifications on the setup are used to evaluate the adaptability to unseen new scenarios, which is tackled through different User Preference configurations. In the

Table 3
Controller solutions for every axis in each case study scenario, together with their corresponding value of user preference term (f_S^{User}) and limit control effort ($u_{\max}$).

Axis	f_s^{User}	$u_{\max}$ [N/kg]	$K_{\max}$ [N/m]	$K_{\min}$ [N/m]	D [N·s/m]
X	6.14×10^{-4}	9.38	4912	1181	128
Y	1.52×10^{-3}	4.69	4861	1169	160
Z	1.24×10^{-3}	4.86	5060	1241	158
(a) Nominal Scenario Controllers: Similarity = 0.3, Scale = 0.5					
Axis	$f_s^{\text{Perf.}}$	$u_{\max}$ [N/kg]	$K_{\max}$ [N/m]	$K_{\min}$ [N/m]	D [N·s/m]
X	2.22×10^{-4}	9.39	4934	4262	138
Y	1.08×10^{-3}	4.16	4989	4130	184
Z	3.78×10^{-2}	0.4	4646	4621	428
(b) Idler Pulley Scenario Controllers: Similarity = 0.9, Scale = 0.5					
Axis	$f_s^{\text{Perf.}}$	$u_{\max}$ [N/kg]	$K_{\max}$ [N/m]	$K_{\min}$ [N/m]	D [N·s/m]
X	2.75×10^{-3}	12.46	8674	2067	183
Y	2.75×10^{-2}	8.15	8081	2089	208
Z	2.01×10^{-2}	8.5	8148	1874	205
(c) Stiffer Belt Scenario Controllers: Similarity = 0.3, Scale = 0.9					

first scenario an idler pulley is introduced (depicted also in Figure 8b), and in the second one the belt used in the nominal scenario is substituted by a stiffer one. Note that the objective of this Section is to evaluate how controller behaviour can be modified according the User Preference heuristic in a real scenario, taking into account that results in Sect. 6 show that introducing safety conditions ensures the generation of reliable controllers.

Independent VICs are used for the translation control of the robot end-effector, namely in X, Y and Z-axis, while orientation ICs remain as in validation experiments (Table 1). The H-GP models are obtained using 10 human guided demonstrations looping the belt on the nominal setup, starting from random initial conditions within an interval. Figure 9a shows obtained reference trajectory together with used demonstrations, and Figs. 9b-d show the compliance ($\lambda(t)$) profile for X, Y

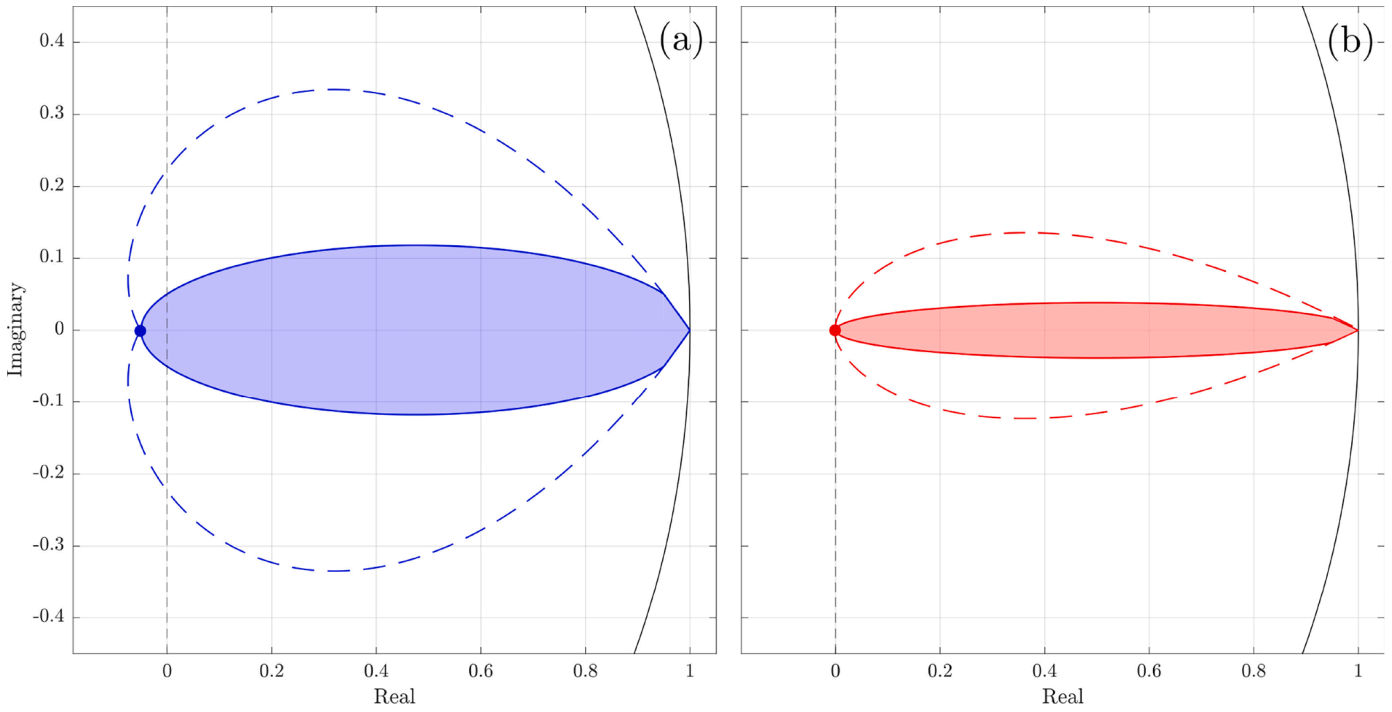

Fig. A1. Representation of the $\mathbb{D}$-stability region (shaded) approximating the non-convex cardioid defined by the logarithmic spirals (dotted-lines) region in the complex plane generated for maximum percentage overshoots of 5% (a) and 0.01% (b).

Table 4
Number of iterations until convergence for each User Preference - LMI Design combination.

Design User Pref.	I	II	III	IV
A	167	170	263	419
B	229	208	322	576
C	156	157	272	504
D	180	176	415	630

and *Z*-axis, respectively. In all Figs. 9a-d task is divided into a set of regions (A to E) based on compliance profiles evolution, as detailed on their caption.

The automated VIC generation definition is given from the same considerations from validation experiments. Hence, the values of $\Delta p_{\max}$ correspond to the minimum difference between the 95% confidence bounds and reference trajectory from the H-GP model, which are 3.12 cm for *X*-axis, 2.03 cm for *Y*-axis and 0.55 cm for *Z*-axis. Note that the same Scale and Similarity values are used for all axis in order to ease interpretation of the results. Thus, controller solutions on Table 3 are obtained, and the results of their execution in the real platform are depicted in Fig. 10. Recalling the aim of using VIC to reduce belt stress during the looping task, the accumulated force exerted on the end-effector along all the directions is represented. A video with all the executions using generated VICs is available as supplementary material and can be also found in the dedicated webpage[4].

7.1. Nominal scenario

In this scenario, no changes are made from the setting used in task demonstrations. Thus, the objective is to find a variable impedance controller solution that reduces the overall force required to perform the task. For this initial setup, we have chosen a Scale value of 0.5 to obtain a maximum stiffness value in the middle of allowed range, and a Similarity value of 0.3 to emphasize the effect of variant behaviour, i.e. increase the difference between K_{max} and $K_{\min}$. As it can be seen in Fig. 10a-c, in all three axis, mean accumulated force is reduced w.r.t. the constant controller strategy between a 9% (*X*-axis) and a 14% (*Z*-axis). Looking at the normalized force difference, it can be seen how stiffness modulation alters the exchanged force along the task. In the first Region, the difference increases in all axis as the stiffness remains low, even though within the first two seconds the variant controller exerts higher forces in *Y*-axis (Fig. 10b) and *Z*-axis (Fig. 10c) than w.r.t. the variant approach (min. of -0.1), which might be an effect of the simultaneous control of position and orientation [5]. Then, in Region B, stiffness increase in *X*-axis does not present a noticeable effect in the force difference, but the same phenomena in *Z*-axis produces a reduction of the difference in Region C for all the axis, as the controller becomes stiffer for the end-effector to reach the desired height. At this point, it is worth remarking that the stiffness regulation in each axis propagates to all the other ones as they all affect the belt elongation. In Region D, stiffness peak in *Y*-axis maintains force difference in all axis, i.e. the controller holds stiff to maintain the position in *Y* at the cost of increasing exchanged force. Finally, accumulated force difference rises as a result of the stiffness reduction in all axes at Region E.

7.2. Idler pulley scenario

The first one-off modification consists on introducing a complementary pulley that provides tension and guides the belt, namely idler. It is positioned next to one of the pulleys where belt is looped before starting the task execution (Fig. 8b), and so the belt also makes contact with it from the beginning. The first approach is to use the same controller as in the nominal scenario, but, although the task can be accomplished, the belt slides over the upper face of the pulley when lowering the end-effector to the desired height (Fig. 11a). This takes

[5] Simultaneously controlling orientation and position might concur in some deviation from the desired behaviour from one in the other, as reported in Dietrich et al. (2021). In this case, the constant impedance controller for orientation could be implemented by imposing its behaviour over the variable one when its stiffness is lower, which can be accentuated due to the initial acceleration caused by the non-zero velocity.

place between Regions C and D (7-7.5 s), just before reaching the maximum stiffness in *Y*-axis. This means that the VIC does not convey enough force to reach a position in *Y*-axis that avoids belt sliding over the pulley. Therefore, from the nominal User Preference, Similarity is increased to 0.9 such that the minimum stiffness gets closer to the maximum one, i.e. a high rigidity is maintained from the beginning of the task. Applying new VICs, task is performed without any issue and the mean accumulated force in all three axis is reduced to values around 20%. Note that the normalized force difference profile has a more uniform behaviour along the task in comparison with the nominal scenario. This means that the behaviour is closer to an equivalent (in the same range of values) constant controller, due to the high Similarity between K_{min} and K_{max}.

7.3. Stiffer belt scenario

For the second scenario, a stiffer belt w.r.t. the nominal one is used. As it can be seen in Fig. 11b, VICs generated for the nominal scenario are not able to fulfil the task. Due to the additional rigidity of the stiffer belt, the controller does not provide enough effort to reach the required position before lowering to the desired height and the looping movement is not performed. This happens just after the stiffness peak in *X*-axis (6-6.5 s), which means that even the maximum stiffness is not enough to counteract the forces from the stiffer belt. Hence, from the nominal User Preference, Scale is increase to 0.9 such that greater values of both K_{max} and K_{min} obtained. This new set of VICs is able to complete the task while reducing the mean accumulated force to values from an 8% (*X*-axis) to a 17.5% (*Z*-axis). The normalized force difference profiles are akin to the nominal scenario ones as both have the same Similarity value. This can be explained through the ratio between maximum and minimum stiffness, which can be seen on Tables 3 a and 3 c to be approx. 4 in all axes. Note also that, w.r.t. nominal scenario, the negative difference in the first two seconds (Figs. 10h,i) is reduced to a min. of -0.05. This might be due to the higher values at the lower stiffness region, which make the VICs less prone to cross-effects from the simultaneous (constant) IC used for orientation.

8. Conclusions and Future Work

This paper presents an approach to set conditions on VICs defined through LfD techniques by the off-line tuning of the parameters that complete its description. Hence, using the approach proposed in Calinon et al. (2010), a time-variant compliance profile from a set of human-guided task demonstrations is used to determine the stiffness term modulation of the VIC. A solution-search method provides sets of parameter values, namely controller solutions, that are assessed in terms of safety and performance conditions. In this work, first ones are stability, limits on position error and control effort, and maximum overshoot (percentage) in the transient response, which are formulated as LMIs on the polytopic description of the VIC. Regarding performance, the User Preference mechanism allows to assess controller solution w.r.t. user intuition over the task, formalised through an heuristic described by Similarity and Scale. This assessment is formulated to provide a compound suitability index for each controller solution, to be used by the solution-search method in the next iterations. Iteratively repeating this process leads to the most suitable controller solution to define the VIC used in task execution.

Validation results in simulation show that generated solutions define VICs that (*i*) fulfil safety conditions, i.e. they are stable, do not surpass design limits on position error and reduce the oscillatory behaviour in the transient response w.r.t. solutions from relaxed assessments, and (*ii*) reflect a compliant behaviour in line with the inputs to User Preference mechanism that conforms performance assessment. In the case study scenario where a real manipulator is used to loop a belt over a pulley (*i*) using generated VICs reduces the accumulated total force required to perform the task in all the settings as (*ii*) User Preference mechanism allows to generate different solutions for the same control architecture fulfilling the same conditions without new task demonstrations.

Future works will explore how extracted task information can be introduced in the form of LMI constraints, e.g. in the form of LQRs as in Calinon et al. (2014), or the application of this method for other LfD approaches, e.g. those that exploit exerted force in human-guided demonstrations to perform position-constrained tasks as in Abu-Dakka et al. (2018). Also, controller assessment will be further extended, mainly in the form of LMI constraints, e.g. introducing passivity for human-interaction tasks Stramigioli (2015). Other extensions of the framework such as the multi DoF case using correlation between demonstrations or the on-line implementation will be also addressed in future works.

Declaration of Competing Interest

The authors declare the following financial interests/personal relationships which may be considered as potential competing interests:

Alberto San-Miguel reports financial support was provided by Spanish State Agency of Research. Alberto San-Miguel reports financial support was provided by European Union.

Acknowledgements

This work is partially supported by MCIN/ AEI /10.13039/ 501100011033 and by the "European Union NextGenerationEU/PRTR" under the project ROB-IN (PLEC2021-007859); and by MCIN/ AEI /10.13039/ 501100011033, Spain, under the project CHLOE-GRAPH (PID2020- 119244GB-I00). Authors also want to thank Adriá Colomé and Edoardo Caldarelli for their comments and help throughout this work.

Appendix A. Proofs of LMI constraints

A1. Proof of Proposition 1

According to Lyapunov theory, the equilibrium point $\mathbf{x}(k) = \mathbf{0}$ is stable if there exists a discrete-time candidate function $V(\mathbf{x}(k))$ such that $\forall k \geq 0$: (*i*) $V(\mathbf{x}(0)) = 0$; (*ii*) $V(\mathbf{x}(k)) \geq 0$, $\forall \mathbf{x}(k) \neq 0$; and (*iii*) $V(\mathbf{x}(k+1)) - V(\mathbf{x}(k)) \leq 0 \, \forall \mathbf{x}(k) \neq 0$. Applying the LMI approach for a generic quadratic candidate function

$$V(\mathbf{x}(k)) = \mathbf{x}(k)^T \cdot \mathbf{P} \cdot \mathbf{x}(k),$$

from condition (iii), conditions (i) and (ii) fulfilled iff there exist a solution matrix $\mathbf{P} = \mathbf{P}^T > \mathbf{0}$ such that the LMI holds:

$$\mathbf{A}(k) \cdot \mathbf{P} \cdot \mathbf{A}(k)^T - \mathbf{P} \leq \mathbf{0} \tag{25}$$

Considering the polytopic description 11, it is proved that the set of matrices $\mathbf{A}(k)$ is positive definite iff matrices from the polytopic description $\mathbf{A}_i$ are positive definite Amato et al. (2005). Hence, definition (25) can be stated as (12), which implies that that solution $\mathbf{P}$ is common to all the vertex state matrices $\mathbf{A}_i$. ■

A2. Proof of Proposition 2

Following Koth et al. (1996), considering solution matrix $\mathbf{P} = \mathbf{P}^T > \mathbf{0}$ that shapes an invariant ellipsoid $\mathscr{E} =: \{\mathbf{z} \,|\, \mathbf{z}^T \cdot \mathbf{P} \cdot \mathbf{z} < \mathbf{I}\}$ and its inverse $\mathbf{Y}$, and the intermediate variable $\mathbf{L} = \mathbf{W}(k) \cdot \mathbf{Y}$, condition (13a,b a) can be stated through the maximum norm of the control effort:

$$\begin{aligned} \| u(k) \|_2^2 &\leq \max_{k \geq 0} \| u(k) \|_2^2 = \max_{k \geq 0} \| \mathbf{L} \cdot \mathbf{Y}^{-1} \cdot \mathbf{x}(k) \|_2^2 \\ &\leq \max_{\mathbf{z} \in \mathscr{E}} \| \mathbf{L} \cdot \mathbf{Y}^{-1} \cdot \mathbf{x} \|_2^2 = \overline{\lambda}\left(\mathbf{Y}^{-1/2} \cdot \mathbf{L}^T \cdot \mathbf{L} \cdot \mathbf{Y}^{-1/2}\right) \leq u_{max}^2 \end{aligned}$$

Thus,

$$\mathbf{L} \cdot \mathbf{Y}^{-1} \cdot \mathbf{L}^T - u_{\max}^2 \leq 0$$

which according the Schur lemma (App. A.4) is equivalent to

$$\begin{bmatrix} u_{\max}^2 \cdot \mathbf{I}_{\mathbf{W}} & \mathbf{L} \\ \mathbf{L}^T & \mathbf{Y} \end{bmatrix} \geq \mathbf{0}$$

Pre/post-multiplying this LMI by the block diagonal matrix $\mathbf{diag}(1, \mathbf{P})$, leads to (14a,b a) considering the definition of $\mathbf{L}$ and the implications of the polytopic description 11, i.e. that set of matrices $\mathbf{W}(k)$ is positive definite iff matrices from the polytopic description $\mathbf{W}_i$ are positive definite Amato et al. (2005).

Similarly, for operational constraint (13a,b b), introducing output equation

$$e(k) = \mathbf{S} \cdot \mathbf{x}(k) \tag{27}$$

leads to

$$\begin{aligned} \| e(k) \|_2^2 &\leq \max_{k \geq 1} \|e_k\|_2^2 = \max_{k \geq 1} \| \mathbf{S} \cdot \mathbf{A} \cdot \mathbf{x}(k-1) \|_2^2 \\ &\leq \max_{\mathbf{z} \in \mathscr{E}} \| \mathbf{S} \cdot \mathbf{A} \cdot \mathbf{z} \|_2^2 = \overline{\lambda}\left(\mathbf{Y}^{1/2} \cdot (\mathbf{S} \cdot \mathbf{A})^T (\mathbf{S} \cdot \mathbf{A}) \cdot \mathbf{Y}^{1/2}\right) \leq \Delta p_{\max}^2 \end{aligned}$$

Thus,

$$(\mathbf{S} \cdot \mathbf{A}) \cdot \mathbf{Y} \cdot (\mathbf{S} \cdot \mathbf{A})^T - \Delta p_{\max}^2 \leq \mathbf{0}$$

which according the Schur lemma (App. A.4) is equivalent to

$$\begin{bmatrix} \mathbf{Y}^{-1} & \mathbf{A}^T \cdot \mathbf{S}^T \\ \mathbf{S} \cdot \mathbf{A} & \Delta p_{\max}^2 \end{bmatrix} \geq 0$$

This LMI leads to (14a,b b) considering the implications of the polytopic description 11, i.e. that set of matrices $\mathbf{A}(k)$ is positive definite iff matrices from the polytopic description $\mathbf{A}_i$ are positive definite Amato et al. (2005). Finally, the initial state $\mathbf{x}(0)$ belongs to the invariant ellipsoid $\mathscr{E}$ iff

$$\mathbf{x}(0)^T \cdot \mathbf{Y}^{-1} \cdot \mathbf{x}(0) - 1 \leq 0$$

which according the Schur lemma (App. A.4) is equivalent to

$$\begin{bmatrix} 1 & \mathbf{x}(0)^T \\ \mathbf{x}(0) & \mathbf{Y} \end{bmatrix} \geq \mathbf{0}$$

Pre/post-multiplying this LMI by the block diagonal matrix $\mathbf{diag}(1, \mathbf{P})$ leads to constraint (15). ■

A3. Proof of Proposition 3

Condition (16) corresponds to the $\mathbb{D}$-stability definition Peaucelle et al. (2000), which is a generalisation of the Lyapunov stability to limit the eigenvalues of state matrix $\mathbf{A}(k)$ to a region $\mathbb{D}$ in the complex plane symmetric w.r.t. real axis and defined through $\boldsymbol{\alpha}$ and $\boldsymbol{\beta}$. A maximum percentage overshoot w.r.t. a reference value $\overline{OS}$ in second order systems corresponds to a maximum damping ratio $\boldsymbol{\xi}$ as defined in (18a a). This corresponds in the (discrete) complex plane to a logarithmic spiral, characterised by φ, which determines its intersection with the real axis a_0 as defined in Eqs. (18a b,c). In Rosinová and Hypiusová (2019), the non-convex region (namely cardioid) generated by these spirals is approximated by the intersection of two regions: an ellipsoid and a cone, defined in Eqs. (18a a,b) and (18a c,d) respectively. The ellipsoid is defined by its center a_{se} (Eq. (18a d)) and its major

and minor axes a_e (Eq. (18a e)) and b_e (Eq. (18a f)); and the cone with its vertex in (1,0) by half its inner angle γ (Eq. (18a g)). To define both regions, an intersection point between them $r = (a,b)$must be specified such that it belongs to the logarithmic spiral. In this paper, a value of $a = 0.95$ has been chosen as it has been seen to provide a good approximation closer to (0,1). Figure A.12 depicts the cardioid regions and their approximations for different $\overline{OS}$ values. ■

A4. Schur Lemma Duan and Yu (2013)

Let the partitioned matrix:

$$\mathbf{M} = \begin{bmatrix} \mathbf{M}_{11} & \mathbf{M}_{12} \\ \mathbf{M}_{12}^T & \mathbf{M}_{22} \end{bmatrix} \geq \mathbf{0}$$

be symmetric. Then,

$$\begin{aligned} \mathbf{M} \geq \mathbf{0} \quad &\Longleftrightarrow \mathbf{M}_{11} \geq \mathbf{0}, \quad \mathbf{M}_{12}^T \cdot \mathbf{M}_{11}^{-1} \cdot \mathbf{M}_{12} - \mathbf{M}_{22} \leq \mathbf{0} \\ &\Longleftrightarrow \mathbf{M}_{22} \geq \mathbf{0}, \quad \mathbf{M}_{12} \cdot \mathbf{M}_{22}^{-1} \cdot \mathbf{M}_{12}^T - \mathbf{M}_{11} \leq \mathbf{0} \end{aligned}$$

Appendix B. Implementation details

Controller design process has been carried out within MATLAB environment using R2109b version on an Intel Core i7-9700K CPU @3.70GHz × 8 with a NVIDIA GP106 GPU.

B1. H-GP model generation

Using the available GP implementation in MATLAB, we consider for the H-GP model generation as convergence criterion an improvement between iterations below 5% w.r.t the difference between the two noise prediction means. Thus, for the validation experiment, using a set of 10 taught position trajectories consisting on 240 samples each (i.e. a sampling time of 0.02 s), the method takes (on average) 9 iterations to converge, which corresponds to an average time of 45.136 s (for each DoF).

B2. Controller solution search

The *off-the-shelf* Bayesian Optimisation Algorithm from MATLAB has been used as the solution-search method. For convergence criterion, we have considered $\epsilon = 0.01$ (below 1% for the fitness range [0,1]) and $N_{\text{iter}} = 75$. The LMI problem has been formulated through the YALMIP toolbox [6] (release $2018-10-12$), and solved with the semi-definite programming algorithms provided by MOSEK [7](version 9.3.10). Thus (on average) each iteration takes 1.737 s from which the generation of the LMI constraints 0.028 s (1.6%), the execution through YALMIP 0.0570 s (3.28%) and MOSEK solver 0.005 s (0.3%). This means that a problem setting that requires 250 iterations for convergence will take approx 7.3[min]. The average number of iterations until convergence for all the User Preferences and Designs used in the validation are included in Table 4.

Supplementary material

Supplementary material associated with this article can be found, in the online version, at 10.1016/j.conengprac.2023.105658

References

Abu-Dakka, F. J., & Kyrki, V. (2020). Geometry-aware Dynamic Movement Primitives. *Proceedings of IEEE International Conference on Robotics and Automation*, (2), 4421–4426. https://doi.org/10.1109/ICRA40945.2020.9196952

Abu-Dakka, F. J., Rozo, L., & Caldwell, D. G. (2018). Force-based variable impedance learning for robotic manipulation. *Robotics and Autonomous Systems, 109*, 156–167. https://doi.org/10.1016/j.robot.2018.07.008

Amato, F., Garofalo, F., & Glielmo, L. (2005). Polytopic coverings and robust stability analysis via lyapunov quadratic forms. *Variable structure and Lyapunov control*, 269–288.

Apkarian, P., Gahinet, P., & Becker, G. (1995). Self-scheduled h-∞ control of linear parameter-varying systems: a design example. *Automatica, 31*(9), 1251–1261.

Bednarczyk, M., Omran, H., & Bayle, B. (2020a). Model Predictive Impedance Control. *Proceedings - IEEE International Conference on Robotics and Automation*, (1), 4702–4708. https://doi.org/10.1109/ICRA40945.2020.9196969

Bednarczyk, M., Omran, H., & Bayle, B. (2020b). Passivity filter for variable impedance control. *2020 IEEE/RSJ international conference on intelligent robots and systems (IROS)* (pp. 7159–7164). IEEE.

Behal, A., Dixon, W., Dawson, D. M., Xian, B., et al. (2009). *Lyapunov-based control of robotic systems*. CRC Press. https://doi.org/10.1201/9781420006278

Calinon, S., Bruno, D., & Caldwell, D. G. (2014). A task-parameterized probabilistic model with minimal intervention control. *2014 IEEE international conference on robotics and automation (ICRA)* (pp. 3339–3344). IEEE.

Calinon, S., Sardellitti, I., & Caldwell, D. G. (2010). Learning-based control strategy for safe human-robot interaction exploiting task and robot redundancies. *Proceeding of IEEE/RSJ International Conference on Intelligent Robots and Systems*, 249–254. https://doi.org/10.1109/IROS.2010.5648931

Dietrich, A., Wu, X., Bussmann, K., Harder, M., Iskandar, M., Englsberger, J., Ott, C., Albu-Schäffer, A., et al. (2021). Practical consequences of inertia shaping for interaction and tracking in robot control. *Control Engineering Practice, 114*(March), 104875. https://doi.org/10.1016/j.conengprac.2021.104875

Duan, G.-R., & Yu, H.-H. (2013). *LMIs in Control Systems*. CRC Press. https://doi.org/10.1201/b15060

Ferraguti, F., Secchi, C., & Fantuzzi, C. (2013). A tank-based approach to impedance control with variable stiffness. *Proceedings - IEEE International Conference on Robotics and Automation*, 4948–4953. https://doi.org/10.1109/ICRA.2013.6631284

Hogan, N. (1985). Impedance control-an approach to manipulation. i-theory. II-implementation. III-applications. *ASME Journal of Dynamic Systems and Measurement Control B, 107*, 1–24.

Ikeura, R., & Inooka, H. (1995). Variable impedance control of a robot for cooperation with a human, *vol. 3. Proceedings of IEEE international conference on robotics and automation* (pp. 3097–3102). IEEE.

[6] YALMIP toolbox : https://yalmip.github.io/

[7] MOSEK softw: https://www.mosek.com

Kersting, K., Plagemann, C., Pfaff, P., & Burgard, W. (2007). Most likely heteroscedastic gaussian process regression. *Proceedings of the 24th international conference on machine learning* (pp. 393–400).

Khader, S. A., Yin, H., Falco, P., & Kragic, D. (2020). Stability-guaranteed reinforcement learning for contact-rich manipulation. *IEEE Robotics and Automation Letters, 6*(1), 1–8.

Khansari, M., Kronander, K., & Billard, A. (2014). Modeling robot discrete movements with state-varying stiffness and damping: A framework for integrated motion generation and impedance control. *Robotics: Science and systems x*. Robotics: Science and Systems Foundation. https://doi.org/10.15607/RSS.2014.X.022

Kober, J., Bagnell, J. A., & Peters, J. (2013). Reinforcement learning in robotics: A survey. *The International Journal of Robotics Research, 32*(11), 1238–1274.

Koth, M. V., Balakrishnan, V., & Morari, M. (1996). Robust constrained model predictive control using linear matrix inequalities. *Automatica, 32*(10), 1361–1379.

Kronander, K., & Billard, A. (2016). Stability Considerations for Variable Impedance Control. *IEEE Transactions on Robotics, 32*(5), 1298–1305. https://doi.org/10.1109/TRO.2016.2593492

Kwiatkowski, A., Boll, M. T., & Werner, H. (2006). Automated generation and assessment of affine LPV models. *Proceedings of the IEEE Conference on Decision and Control*, (2), 6690–6695. https://doi.org/10.1109/cdc.2006.377768

Medina, J. R., Lee, D., & Hirche, S. (2012). Risk-sensitive optimal feedback control for haptic assistance. *2012 IEEE international conference on robotics and automation* (pp. 1025–1031). IEEE.

Peaucelle, D., Arzelier, D., Bachelier, O., & Bernussou, J. (2000). A new robust d-stability condition for real convex polytopic uncertainty. *Systems & control letters, 40*(1), 21–30.

Ravichandar, H., Polydoros, A. S., Chernova, S., & Billard, A. (2020). Recent advances in robot learning from demonstration. *Annual review of control, robotics, and autonomous systems, 3*, 297–330.

Rosinová, D., & Hypiusová, M. (2019). LMI pole regions for a robust discrete-time pole placement controller design. *Algorithms, 12*(8). https://doi.org/10.3390/a12080167

San-Miguel, A., Alenyà, G., & Puig, V. (2022). Automated off-line generation of stable variable impedance controllers according to performance specifications. *IEEE Robotics and Automation Letters, 7*(3), 5874–5881.

Shamma, J. S. (2012). An overview of LPV systems. *Control of linear parameter varying systems with applications* (pp. 3–26). Springer.

Stramigioli, S. (2015). Energy-aware robotics. *Mathematical control theory i* (pp. 37–50). Springer.

Sun, X.-D., & Postlethwaite, I. (1998). Affine LPV modelling and its use in gain-scheduled helicopter control. *Ukacc international conference on control'98 (conf. publ. no. 455)* (pp. 1504–1509). IET.

Toth, R., Heuberger, P. S. C., & Van den Hof, P. M. J. (2010). Discretisation of linear parameter-varying state-space representations. *IET control theory & applications, 4*(10), 2082–2096.

Yokokohji, Y., Kawai, Y., Shibata, M., Aiyama, Y., Kotosaka, S., Uemura, W., Noda, A., Dobashi, H., Sakaguchi, T., & Yokoi, K. (2019). Assembly challenge: a robot competition of the industrial robotics category, world robot summit–summary of the pre-competition in 2018. *Advanced Robotics, 33*(17), 876–899.